MELT FLOW CONTROL IN THE DIRECTIONAL SOLIDIFICATION OF BINARY ALLOYS

Nicholas Zabaras*

Materials Process Design and Control Laboratory
Sibley School of Mechanical and Aerospace Engineering
188 Frank H. T. Rhodes Hall
Cornell University, Ithaca, N.Y. 14853-3801, U.S.A.

Our main project objectives are to develop computational techniques based on inverse problem theory that can be used to design directional solidification processes that lead to desired temperature gradient and growth conditions at the freezing front at various levels of gravity. It is known that control of these conditions plays a significant role in the selection of the form and scale of the obtained solidification microstructures.

Emphasis is given on the control of the effects of various melt flow mechanisms on the local to the solidification front conditions. The thermal boundary conditions (furnace design) as well as the magnitude and direction of an externally applied magnetic field are the main design variables. We will highlight computational design models for sharp front solidification models and briefly discuss work in progress toward the development of design techniques for multi-phase volume-averaging based solidification models.

Model Description

Let us introduce a model directional solidification problem of a dilute, incompressible, electrically conducting binary alloy in a two-dimensional rectangular enclosure with an open boundary (Fig. 1). At time t = 0$^+$, a cooling heat flux is applied on the mold boundary Γ_{OS} and solidification commences. Here, we assume a-priori that the growth conditions are such that solidification occurs with a stable solid-liquid interface [1]. This model provides us with the opportunity to concentrate on the melt flow mechanisms and in addition to control interface quantities that are readily available in the direct analysis.

In the following problem definition, the following dimensionless numbers are used [1], [2]: θ (dimensionless temperature) $\equiv (T - T_o)/\Delta T$, Ha (Hartmann number), Le (Lewis number), Ma_T (thermal Marangoni number), Ra_T (thermal Rayleigh number), Ra_C (solutal Rayleigh number), R_α (ratio of thermal diffusivities), R_k (ratio of thermal conductivities) and Ste (Stefan number). The equations governing the various transport mechanisms in the melt in the binary alloy solidification system are

$$\frac{\partial \mathbf{v}}{\partial t} + \mathbf{v} \cdot \nabla \mathbf{v} = -\nabla p + \Pr \nabla^2 \mathbf{v} - [Ra_T \Pr \theta - Ra_c \Pr c]\mathbf{e}_g + Ha^2 \Pr[\mathbf{v} \times \mathbf{e}_B] \times \mathbf{e}_B \quad (1)$$

$$\frac{\partial \theta}{\partial t} + \mathbf{v} \cdot \nabla \theta = \nabla^2 \theta \quad (2)$$

$$\frac{\partial c}{\partial t} + \mathbf{v} . \nabla c = Le^{-1} \nabla^2 c \quad (3)$$

*Corresponding author. E-mail: zabaras@cornell.edu

695

The thermal field distribution in the solid is governed by the heat conduction equation:

$$\frac{\partial \theta_s}{\partial t} = R_\alpha \nabla^2 \theta_s \tag{4}$$
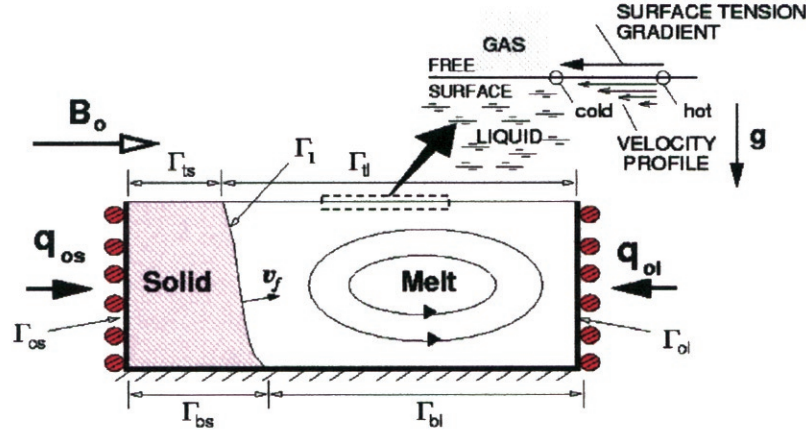
Figure 1: Schematic of the binary alloy solidification problem in an open boat configuration under the influence of an externally applied magnetic field.

The interfacial temperature is determined by the equilibrium phase diagram:

$$\theta = \theta_m + mc \tag{5}$$

where the dimensionless slope m of the liquidus is given as $m=m_{liquidus}\Delta c/\Delta T$, $m_{liquidus}$ is the dimensional slope of the liquidus and θ_m is the dimensionless melting temperature.

The interfacial thermal and solute fluxes are governed by the Stefan condition and the solute conservation condition on the freezing interface:

$$R_k \frac{\partial \theta_s}{\partial n} - \frac{\partial \theta_l}{\partial n} = Ste^{-1}\mathbf{v}_f \cdot \mathbf{l} \tag{6}$$

$$\frac{\partial c}{\partial n} = Le(\kappa - 1)\mathbf{v}_f \cdot n(c+\delta) \tag{7}$$

where the normal vector $\mathbf{n}$ is pointing out from the liquid domain, κ is the partition coefficient and δ ≡ $c_o/\Delta c$ is the ratio of the reference concentration c_o and reference concentration drop Δc.

No-slip and no-penetration boundary conditions are imposed on all surfaces other than the upper free surface. The hydrodynamic condition on Γ_{tl} is of the form:

$$\nabla(\mathbf{v}\cdot\mathbf{t}).n = Ma_T(\nabla\theta\cdot\mathbf{t}) \tag{8}$$

where $\mathbf{t}$, is a tangent vector to the free-surface. Insulating thermal boundary conditions are imposed on the top and bottom boundaries of the solid and liquid domains. Thermal boundary conditions are provided on Γ_{os} and Γ_{ol}. Finally, a solute impermeable condition is imposed on the mold boundaries and the free surface.

The solution scheme implemented uses a front-tracking SUPG/PSPG finite element method with mass lumping and preconditioning [1].

696

Reference Design And Parametric Studies

Before we address computational design solidification problems, it is imperative to provide an understanding of the effects of the various physical mechanisms on the local to the freezing front conditions. A parametric study was performed in this context to investigate the effects of various process parameters.

Let us consider a rectangular cavity with an open free surface of dimensions 2 cm x1 cm initially filled with molten antimony-doped germanium at 40°C overheat (Fig. 1). The wall Γ_{ol} is maintained at the initial temperature, while Γ_{os} is suddenly cooled to a temperature 40°C below the melting temperature of pure germanium and maintained at that temperature for $t > 0$. The thermophysical properties are extracted from [1].

At t=0$^+$ solidification starts and takes place under standard laboratory conditions. We refer to this problem as the *reference design problem*. The results of the *reference design problem* at $\tau = 10$ are shown on the left of Fig. 2.
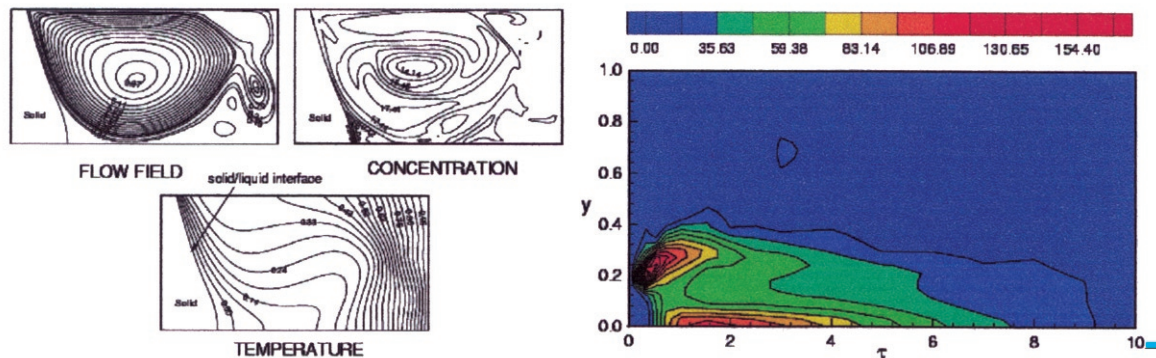
Figure 2: Normal gravity and zero magnetic field conditions for the solidification of SbGe. On the left: Contours of stream function, solute concentration and temperature fields at time $\tau = 10$. On the right: Calculated history of the solid-liquid interface concentration during the entire simulation.

Figure 2 also presents the history of the concentration on Γ_I during the entire simulation. This plot effectively shows the pattern of the solute variation obtained in the final solid. To assess the relative importance of thermocapillary versus buoyancy effects on solidification, a calculation was performed for solidification in a very low-gravity g=10^{-5} g$_{earth}$ environment (Fig. 3) At early times $\tau < 0.5$, thermal gradients on the free surface lead to surface-tension gradients and a thermocapillary flow develops slowly, forming a small counter-clockwise cell around the free surface very close to Γ_I. There is almost no convection in the lower part of the cavity at this time. As the solidification proceeds further, the strength of this recirculating fluid flow slowly increases, along with a steady increase in the size of the cell. Around $\tau = 2$, the main recirculating cell fills almost the entire cavity. At the same time, a secondary cell pattern forms at the right end of the cavity. After around $\tau = 3$ there is almost no change in the structure of the main cell, even though its strength steadily increases with time (Fig. 3 (left)).

This complex evolution of the melt flow has significant impact on various solidification parameters (e.g. compare Figs. 2 (right) and 3 (right)) [1].
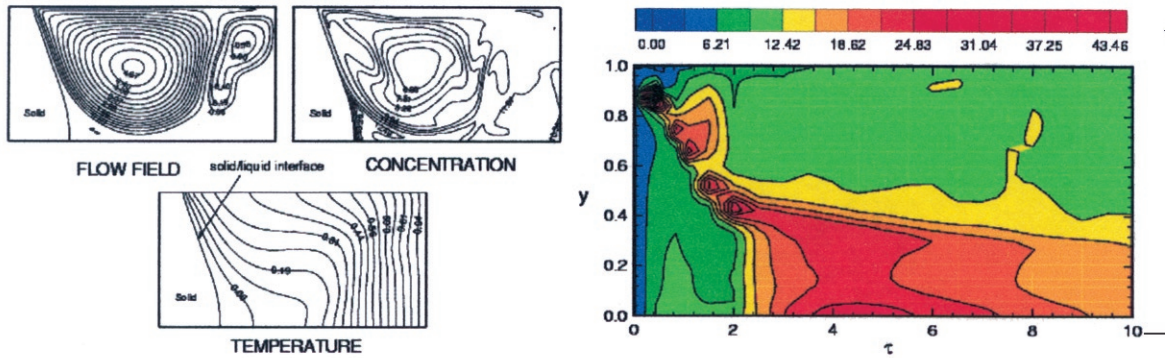
Figure 3: Reduced gravity ($g=10^{-5}$ g_{earth}) conditions and zero magnetic field for the solidification of SbGe. On the left: Calculated contours of stream function, solute concentration and temperature fields at time $\tau = 10$. Notice the significant influence of the flow field on the solute distribution in the melt. On the right: Calculated history of the solid-liquid interface concentration during the entire simulation.

An extensive series of simulations were conducted under various levels of gravity (Fig. 4). These studies have shown that 'flat interface growth' cannot be achieved by a reduced gravity environment and additional means of control are needed. Simulations were also conducted at various inclinations of the magnetic field. Figure 5 shows the variety of flow patterns obtained for various magnetic field inclinations at time $\tau =10$. The prominent effect of varying the orientation of the magnetic field is to drastically alter the structure of the fluid flow especially under reduced gravity conditions.

Finally, Figure 6 illustrates the variety of melt flow patterns obtained by varying the strength of the applied horizontal magnetic field under normal and reduced gravity conditions. An increasing magnetic field damps the melt flow and also has significant impact on the structure of the flow and application of sufficiently high magnetic fields (Fig. 6(c)) leads to separation of the thermocapillary- and buoyancy-driven rolls. As one can note from Fig. 6(f), solidification under reduced gravity and sufficiently strong magnetic field ensures that the solid-liquid interface is almost flat which in fact is one of the objectives of the design problems under consideration. In the following section, we will briefly highlight a design methodology to achieve a desired flat-interface growth that is also ensured to be morphologically stable.

In closure, Fig. 7 compares the solute pattern obtained under normal and reduced gravity conditions with an applied magnetic field. As expected, markedly different transport patterns in the two systems lead to entirely different form of solute segregation. As seen in Fig. 7(a), the maximum solute concentration under normal gravity conditions is seen in the bottom part of the rectangular cavity at very early times. In contrast, Fig. 7(b) shows that the maximum solute collection occurs very near the free-surface and at early times. This trend is in conformity with the fluid flow circulation which is restricted mainly to regions close to the free-surface.

698
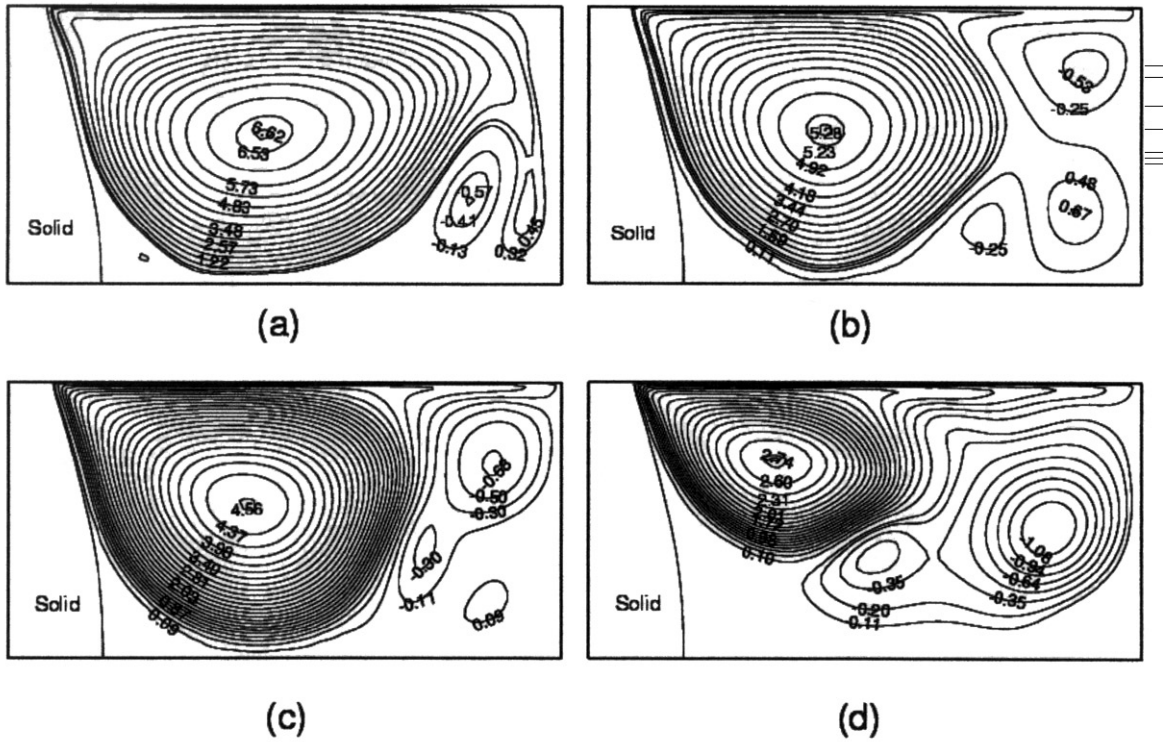
Figure 4: Effects of gravity with no magnetic field: Contours of stream function at time $\tau = 5$ for the solidification of SbGe under varying levels of gravity: (a) $0.5g_{earth}$ (b) $0.1g_{earth}$ (c) $0.01g_{earth}$ (d) $10^{-5}g_{earth}$.

Inverse Design To Achieve A Desired Stable Growth

Using parametric studies to compute the optimal process conditions becomes an expensive and time-demanding process. To alleviate such difficulties, a computational design framework was developed for the thermal design of directional solidification processes. The objective here is to control the mold wall cooling/heating boundary conditions in order to achieve a desired stable interface growth. As a first attempt, the magnitude and orientation of the magnetic field and gravity are a-priori selected based on the parametric studies discussed earlier.

To simplify the design analysis presented here, we assume eutectic solidification with the interfacial temperature of the liquid and solid and composition of the liquid given by

$$\theta_l = \theta_s = \theta_E \quad \text{and} \quad c = c_E \quad \text{on} \quad \Gamma_I(t) \tag{9}$$

The solid composition is determined by the dimensionless mass balance

$$(c_s - c_E)(\mathbf{v}_f . \mathrm{n}) = Le^{-1}\frac{\partial c}{\partial n} \tag{10}$$

With all remaining governing equations as given earlier, we pose the following inverse design problem (see Fig. 8):

Find the cooling heat flux $q_{os}(\mathbf{x}, t)$ on the boundary $\boldsymbol{\Gamma}_{os}$ as well as the heat flux condition $q_{ol}(\mathbf{x}, t)$ on the vertical mold wall $\boldsymbol{\Gamma}_{ol}$ (see Fig. 8a) so that in the presence of coupled thermocapillary, buoyancy and electromagnetically driven convection in the melt, a desired flat-interface growth (with desired flux G and growth velocity $\mathbf{v}_f$) is achieved that is ensured to be morphologically stable.
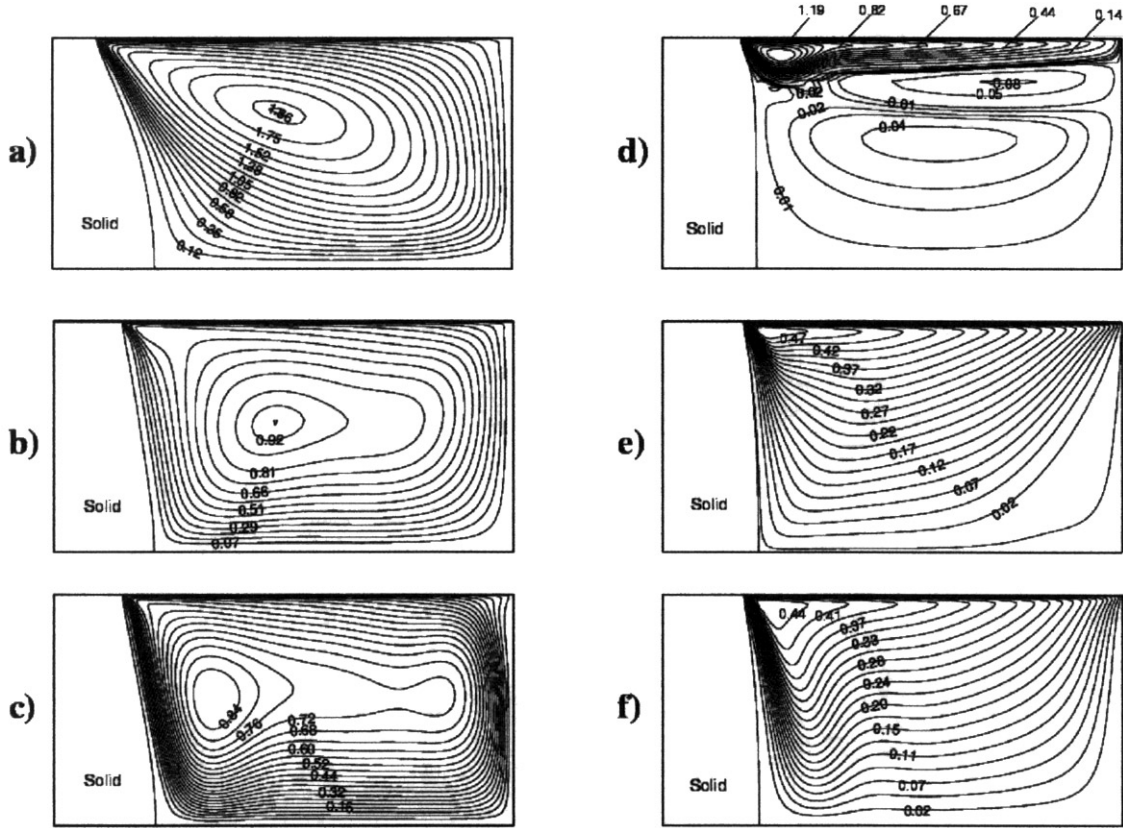
Figure 5: Effect of magnetic field orientation: Calculated contours of stream function at time $\tau = 10$ for the solidification of SbGe under the influence of an externally imposed horizontal magnetic field (Ha=100) at various magnetic field orientations. Solidification under normal gravity conditions: (a) along the x-axis; (b) 60° ccw to the x-axis; (c) along the y-axis, Solidification under reduced-gravity $10^{-5}g_{earth}$ conditions: (d) along the x-axis; (e) 60° ccw to the x-axis; (f) along the y-axis.

The above inverse design problem can be divided into two sub problems, one inverse problem in the solid region and another in the liquid region [3]. This is possible since, as part of the design objectives, the location of the interface Γ_I is explicitly known through the given growth velocity $\mathbf{v}_f$. The inverse problem in the solid domain is the well-studied inverse heat conduction problem. The inverse problem in the liquid domain is depicted in Fig. 8(b) and it involves coupled effects of thermocapillary, buoyancy and electro-magnetic forces [4, 5, 6].

As a first step, in this work, the *constitutional stability criterion* is considered to enforce the morphological stability of the solid-liquid interface. In particular, we consider the following constraint on the G/| $\mathbf{v}_f$| ratio [4],

$$\frac{G}{|\mathbf{v}_f|} \geq \frac{-m_L(c_E - c_o)}{D_L} \tag{11}$$
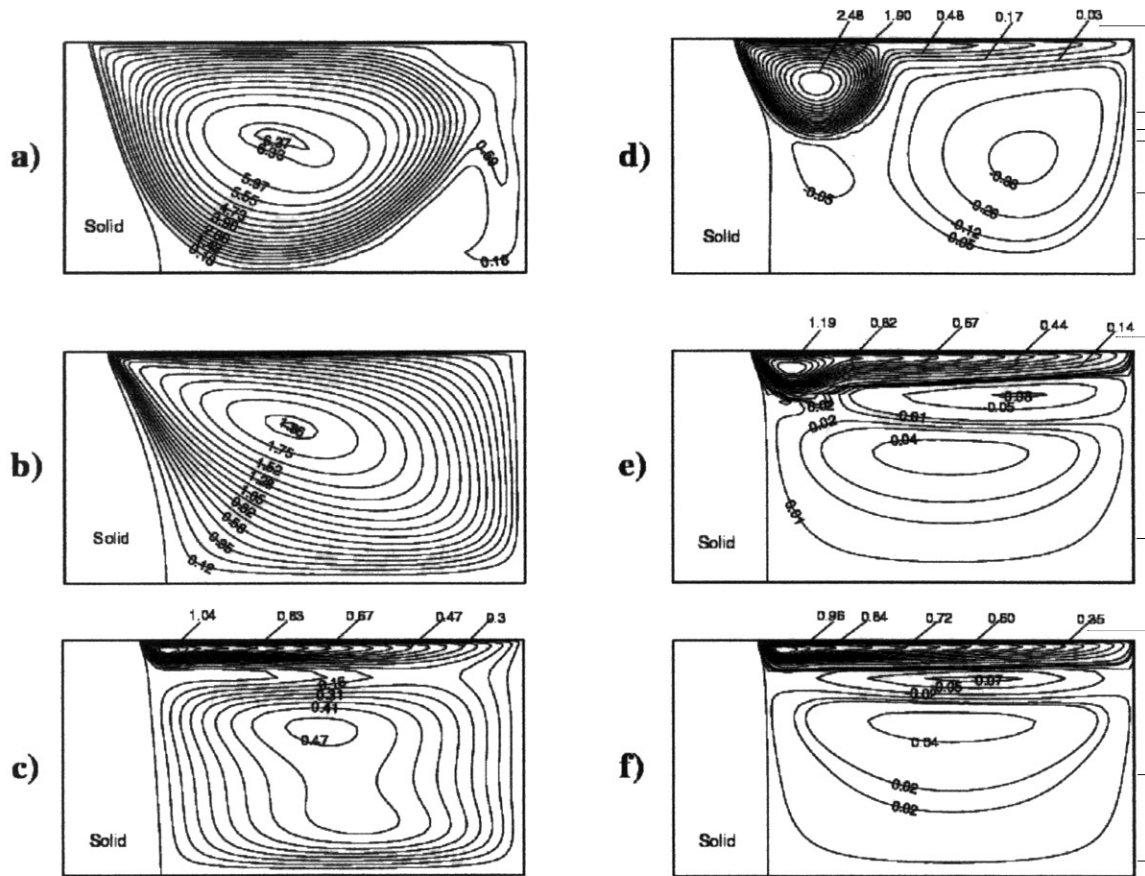
Figure 6: Effect of the magnetic field strength: Calculated contours of stream function at time τ = 10 for the solidification of SbGe. Solidification under normal gravity conditions: (a) Ha=10 (b) Ha=100 (c) Ha=200, Growth under reduced gravity (g = 10^{-5}g$_{earth}$) conditions: (d) Ha=10 (e) Ha=100 (f) Ha=200.
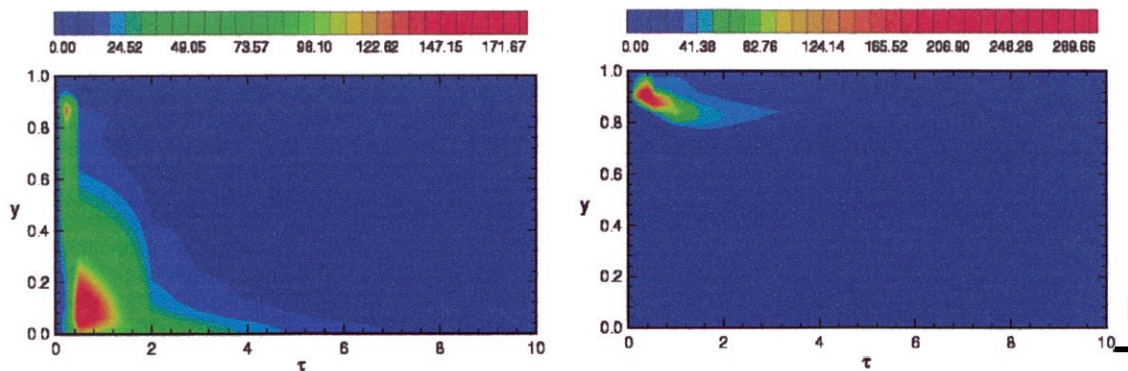
Figure 7: History of the solid-liquid interface concentration during the entire simulation of SbGe solidification for Ha=100: (a) normal gravity conditions; (b) reduced gravity (g=10^{-5} g$_{earth}$) conditions.

to be sufficient to ensure stability of the solid-liquid interface. We herein enforce stability by explicitly choosing an interface thermal gradient G and growth velocity $\mathbf{v}_f$ such that G/| $\mathbf{v}_f$| marginally satisfies the constraint given in equation (11). In our preliminary work, we have chosen $\mathbf{v}_f$ as the growth corresponding to diffusion based process [4].
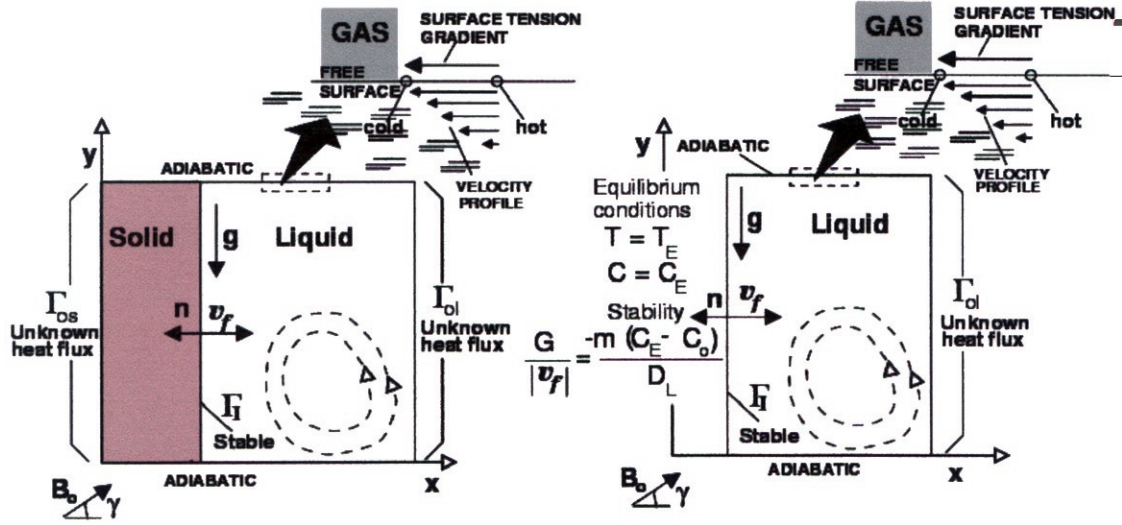
Figure 8: Definition of the design eutectic solidification problem. The design objectives are the achievement of a desired growth v_f under the conditions of marginal stability.

In the following discussion, we present the essentials of the adjoint method for solving the above described inverse design eutectic solidification problem. The space of *admissible controls* is defined as the Hilbert space $U = H^1(\Gamma_{ol} \times [0, t_{max}])$. With a *guessed* heat flux $q_{ol}(x,t)$, $(x,t) \in \Gamma_{ol} \times [0, t_{max}]$, one can define a direct coupled thermocapillary-buoyancy-electromagnetic convection problem on the prescribed domain $\Omega_l(t)$. Let us denote its solution for the temperature, concentration and flow fields as $\theta(x, t; q_{ol})$, $c(x, t; q_{ol})$ and $\mathbf{v}(x, t; q_{ol})$, respectively. The equilibrium condition $\theta(x, t) = \theta_E$, $(x,t) \in \Gamma_I \times [0, t_{max}]$ is not used in this *direct problem* definition, thus it is not guaranteed to be satisfied. For an arbitrary $q_{ol} \in H^1(\Gamma_{ol} \times [0, t_{max}])$, we define a cost functional:

$$\mathcal{J}(q_{ol}) = \frac{1}{2} \| \theta(x,t;q_{ol}) - \theta_E \|^2_{L_2(\Gamma_I \times [0,t_{max}])} + \frac{\gamma}{2} [\| q_{ol} \|^2_{L_2(\Gamma_{ol} \times [0,t_{max}])} + \| \nabla q_{ol} \|^2_{L_2(\Gamma_{ol} \times [0,t_{max}])}] \quad (12)$$

where $\gamma \in \mathfrak{R}^+$ is an appropriate regularization parameter chosen based on the numerical errors in the algorithm. In this paper, our objective is to construct a minimizing sequence $q^k_{ol}(x,t) \in U$, that converges to at least a local minimum of $\mathcal{J}(q_{ol})$.

To perform the optimization procedure that minimizes $\mathcal{J}(q_{ol})$, we will need to define a *continuum sensitivity problem* in terms of the sensitivity velocity field $\hat{V}(x,t;q_{ol})$, sensitivity temperature field $\hat{\Theta}(x,t;q_{ol})$ and sensitivity concentration field $\hat{C}(x,t;q_{ol})$. This linear problem is derived by computing the linear perturbations of the fields $\theta(x,t;q_{ol})$, $c(x,t;q_{ol})$ and $\mathbf{v}(x,t;q_{ol})$, respectively, with respect to the variations $\Delta q_{ol}(x, t)$ of the design heat flux q_{ol} [3]-[8]. In order to realize the minimization of $\mathcal{J}(q_{ol})$, it is essential to find its gradient $\mathcal{J}'(q_{ol})$ with respect to the design flux q_{ol}. An associated *adjoint problem* can be defined in terms of the adjoint velocity field $\tilde{\phi}(x,t;q_{ol})$, adjoint temperature field $\tilde{\psi}(x,t;q_{ol})$, and adjoint concentration field $\tilde{\rho}(x,t;q_{ol})$. The gradient of $\mathcal{J}(q_o)$ with respect to the scalar product $(.,.)_{H^1(\Gamma_{ol} \times [0,t_{max}])} \equiv (.,.)_{L_2(\Gamma_{ol} \times [0,t_{max}])} + (\nabla ., \nabla .)_{L_2(\Gamma_{ol} \times [0,t_{max}])}$ was shown to be given by [5,6]

$$\mathcal{J}'(q_{ol}) = z + \gamma q_{ol} \quad (13)$$

702

where z is the solution of an additional variational equation on Γ_{ol}:

$$-\Delta z(x,t) + z(x,t) = \psi(x,t;q_{ol}) \qquad (14)$$

Thus, to calculate the gradient of the cost functional including an H^1 type regularized formulation, the solution component $\widetilde{\psi}(x,t;q_{ol})$ of the adjoint equations has to be first computed together with the solution z of the above variational problem.

After having obtained an analytical expression for the exact gradient, any of the standard functional minimization techniques can be used for solving the above defined optimization problem such as the non-linear conjugate gradient method (CGM) [6].

Numerical Example In The Design Of Eutectic Solidification
Consider a rectangular cavity with an open free surface of dimensions 20 mm x 20 mm filled with molten Sb - 8.6 wt% Ge, initially at 100°C above the eutectic temperature (592° C). At time $t = 0^+$, the left wall Γ_{os} is suddenly cooled to a temperature 100 °C below the eutectic temperature and maintained at that temperature for times $t > 0$. All other walls are insulated. The thermophysical properties are given in [4].

At $t = 0^+$ the freezing process starts and takes place under standard laboratory conditions. We refer to this problem as the *reference design problem*. In [4] it has been shown that the solution of this reference problem leads to a complex variation of solute in the product and in addition corresponds to a physically unrealistic (unstable) process. A design problem is thus introduced to compute the transient mold walls thermal conditions for the reference eutectic solidification system such that a stable growth is achieved with a growth velocity equal to that of a solidification problem controlled only by heat/solute diffusion. A horizontal magnetic field of Ha = 36.74 is applied. This design example computes process parameters that lead to "diffusion-based" conditions in the presence of convection. We pose the following problem:

Find the thermal boundary conditions on the left wall $\boldsymbol{x} = 0$ *and the right wall* $\boldsymbol{x} = 1$ *such that with coupled thermocapillary, buoyancy, and electromagnetic convection in the melt, a vertical desired interface growth is achieved that is morphologically stable (see Fig. 8).*

The inverse solidification problem can be decomposed into an *inverse heat conduction problem* in the solid and a *inverse convection problem* in the melt (Fig. 8). The inverse problem in the liquid domain solves for $q_{ol}(y, t)$ at x = 1 using the given freezing interface velocity $\mathbf{v}_f(t)$ and the interface thermal gradient G. $\mathbf{v}_f(t)$ is here defined by solving a direct solidification problem without the effects of melt convection and G is chosen using this interface velocity field such that the stability condition is marginally satisfied. An initial guess $q^0{}_{ol}(y, t) \equiv 0$ corresponding to the reference eutectic solidification problem was chosen to start the CGM algorithm. Within each CGM iteration, the direct, adjoint and sensitivity problems are solved using the same finite element algorithms [7].

The development of the heat flux profiles during the intermediate stages of CGM process is shown in Fig. 9. Note that this optimal heat flux profile $\overline{q}_{ol}(y,t)$ shows largest heating at very early times. This strong heating flux has to be applied at early times in order to counteract the effects of coupled thermocapillary and buoyancy-driven fluid flow at the very early stages of the solidification process. It is the combined application of the heat fluxes $\overline{q}_{os}(y,t)$ and $\overline{q}_{ol}(y,t)$, which leads to the desired stable growth conditions.

(a) (b)

(c) (d)
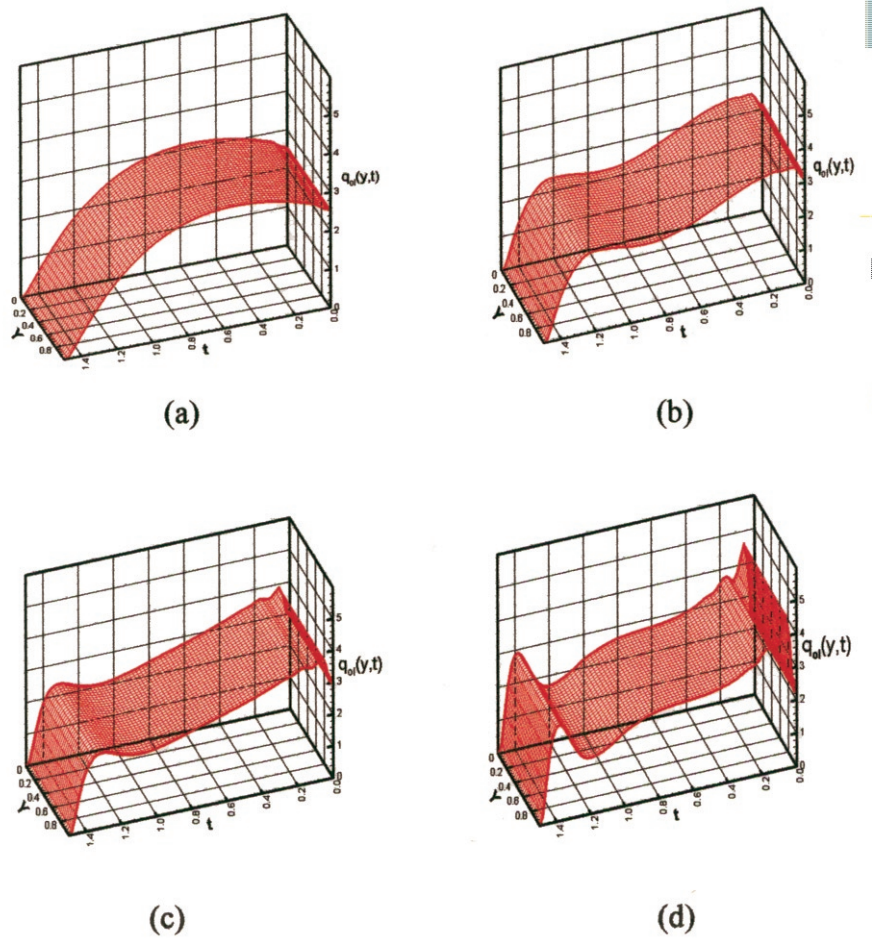
Figure 9: Flux distribution $q^k_{ol}(y, t)$ obtained at CGM iterations k = 1, 2, 5, and 10, starting from an initial guess heat flux $q^0_{ol}(y, t) \equiv 0$. The solution at k=10 is nearly the final optimal solution.

We proceed to evaluate how close the desired design objectives have been met. A direct eutectic solidification problem is considered with the calculated optimal solid side flux $\bar{q}_{os}(y,t)$ applied on the left boundary x = 0 (not shown here) and the liquid side flux $\bar{q}_{ol}(y,t)$ applied on the right boundary x= 1. The top and bottom walls are, as before, insulated. We refer to this problem as the *optimal design eutectic-solidification problem*.

Representative transient temperature, concentration and flow fields corresponding to the optimal design problem are illustrated in Fig. 10. The strong heating flux on the right boundary x = 1 is necessary to overcome the solutal undercooling and maintain a stable interface growth throughout the process. Figure 11(b) shows the dimensionless contours of $\Delta(y, t) \equiv G/|\mathbf{v}_f| + m (C_E - C_o)/D_L$ as a function of the y-coordinate and time. Stable growth $(\Delta(y, t) \geq 0)$ is achieved for the entire duration of solidification confirming the realization of the design objectives. Finally, in Fig. 11(a) note the vertical uniformity in the solid composition in comparison to the stratification observed in the initial design given in Reference [4].

Figure 10: Contours of the fluid stream function (a-c), isotherms (d-f) and composition (g- i) for the optimal design eutectic solidification simulation. Results are shown at times $\tau = 0.1$, $\tau = 0.8$ and $\tau = 1.5$.

Further Developments

We are currently extending the above design algorithms to volume averaging based solidification models with main objectives the control of the solidification conditions within the mushy zone. A continuum sensitivity framework is being developed to allow us to perform gradient-based design optimization problems with the thermal boundary conditions, the level of gravity and the magnetic field being the main design variables. In contrast to the design problems discussed earlier, our design objectives are now defined within the mushy zone where all micro structural features are determined. In between various design problems, we are particularly interested at optimization problems that can be used to control the mushy zone morphology as well as the homogeneity of the solidified product.

Figure 11: (a) The solid composition for the optimal solidification problem. The contours are labeled in wt% Germanium (b) dimensionless contours of $\Delta \equiv G/|\mathbf{v}_f| + m (C_E - C_o)/D_L$ are displayed. Notice that stable growth is achieved for the entire duration of solidification.

References

[1] R. Sampath and N. Zabaras, J. Comp. Physics, **168**, 384--411 (2001).

[2] N. Zabaras, Proceedings of the 2nd Pan-Pacific Basin Workshop on Microgravity Sciences, Pasadena, CA, May 1--4, 2001.

[3] G. Z. Yang and N. Zabaras, *J. Comput. Phys.* **140**, 432--452 (1998).

[4] R. Sampath and N. Zabaras, *Numerical Heat Transfer : Part A*, **39**, 655--683 (2001).

[5] R. Sampath and N. Zabaras, *Int. J. Numer. Meth. Engr.*, **50**, 2489--2520 (2001).

[6] R. Sampath & N. Zabaras, *Comp. Methods Appl. Mech. Engr.*, **190,** 2063--2097 (2001).

[7] R. Sampath and N. Zabaras, *Int. J. Numer. Methods Engr.* **48**, 239--266 (2000).

[8] N. Zabaras, 'Transport Phenomena in Materials Processing', ASME (2001).